Event detection methods for high resolution time measurements on an application example

Rocco Reinhardt, IAV GmbH, Rocco.Reinhardt@iav.de

Olaf Magnor, IAV GmbH

Peter Dünow, Hochschule Wismar

Olaf Hagendorf, Hochschule Wismar

Amelie Rohlfs, IAV GmbH

September 17, 2014

Abstract

The accuracy of high resolution time measurements is influenced negatively by many factors. One key factor of time measurements represents the determination of start and stop events. This paper treats of some of the major factors of event detection. These are the time jitter and the time walk effect. They are analysed and their qualitative impacts of the measurement accuracy are shown.

The referred effects are caused by different signal properties. So the standard deviation of acquired time stamps is adversely affected by variable amplitudes and rise times. Subsequently procedures are shown, which minimise or neutralise these effects. Parts of the investigated methods are variants of leading-edge-discriminators (LED) and constant-fraction-discriminators (CFD).

Based on the former analysis a software implementation of a CFD combined with a high-low-coincidence procedure is presented. This implementation is suitable for offline event detection in data vectors. First application results are presented and interpreted. Finally an outline of different variants follows, which enables a realisation for online analysis.

1 Negative influences of event detection by time measurements

The event detection is of central importance for high resolution time measurements. Dependent on the application four points for the implementation are to be noted: available resources, repeatability, adequate resolution, adequate accuracy.

The event detection is at least influenced by time walk and jitter effects [1]. Particularly the **time walk effect** occurs at constant trigger thresholds, variable signal amplitudes and variable signal rise times. Varying signal amplitudes are very common in

analogue measuring concepts. In figure 1 (a),(b) the sources for time walk effects on a simple linear example are shown. In each plot are three curves. Once with variable amplitudes σ_A but identical rise times T_R and once with variable rise times σ_{T_R} and constant amplitudes A. These result to different slopes from event to event and thus to uncertainty threshold A_{Th} crossings and is termed as σ_T. The time walk effect can be minimised by lowering the trigger threshold, this is limited by noise. At too low thresholds the noise signal would be conditioned to activate the trigger without a valid signal.

(a) Time walk effect caused by variable amplitudes

(b) Time walk effect caused by variable rise times
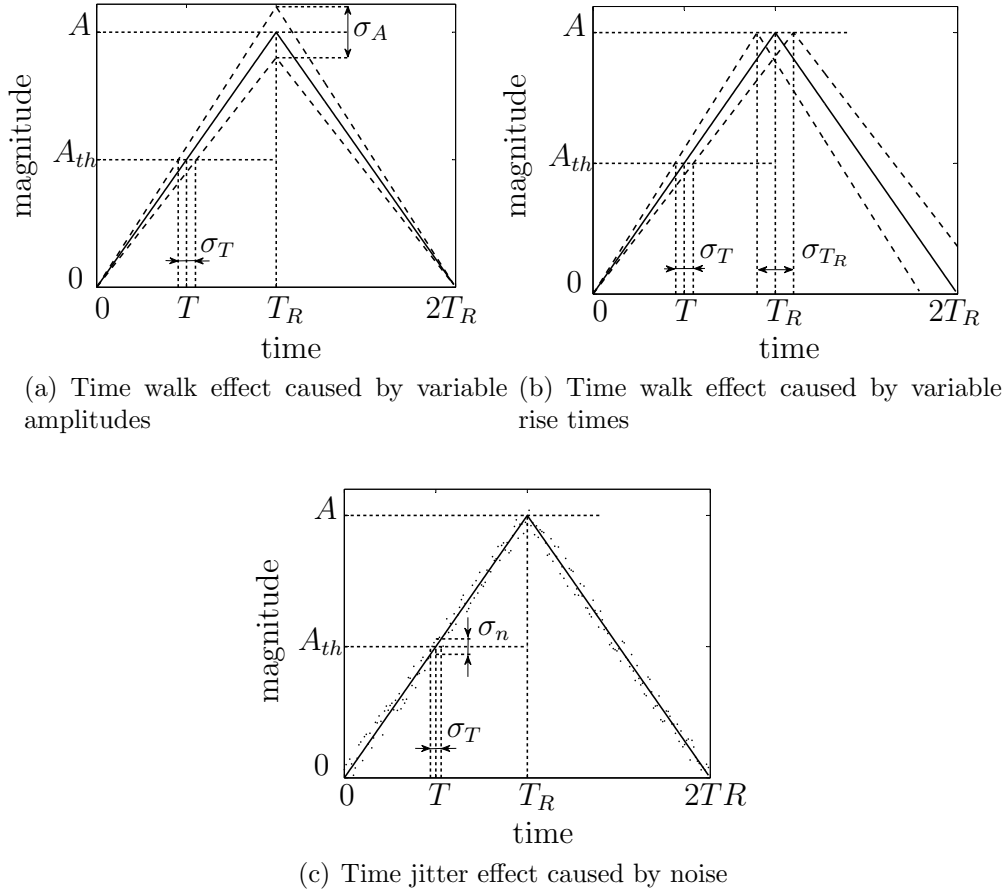

(c) Time jitter effect caused by noise

Figure 1: Influences of time event detection

The **time jitter effect** arises with noise and generates varying threshold crosses because of the stochastic distributed noise amplitudes (figure 1 (c)). It occurs always, however the intensity and influence change. By simple geometrical considerations it becomes obviously, that the slew rate when crossing the threshold has to be as steep as possible to minimise all the described negative effects. For example, a relatively flat signal slope m_T close to the crossing magnitude would cause a wide range of possible detected time events (equation 1, [2]), induced by noise. The effect of the measurement accuracy can be reduced by averaging, but is not always feasible in the desired dimensions. Thus, the time jitter often decreases the quality of a high resolution time measurement system sustained. Further effects on time measurement are described in [1], [2], [3], [4], [5]. In the next chapter a detailed examination of the qualitative influences of different event detection

methods, follows.

$$\sigma_T = \frac{\sigma_n}{m_T} \tag{1}$$

2 Methods to minimise negative influences of event timing by time measurements

There are a few available methods for event detection. These methods can be chosen in subject to signal characteristics, desired measurement accuracy, and available resources.

The standard application for an event detection is the **leading edge discriminator** (LED). In electronics or micro controller environment it is also known as Schmitt-Trigger, which is a comparator with hysteresis. This component shows advantages as to very low prices and simpleness. The trigger threshold is mostly the half supply voltage of the component. The possible signal rise times and amplitudes should be in same dimensions, depending on requirements, due to the lack of mechanisms to minimise failures. For applications with standard accuracy requirements or very good repeatable signal quality, it is the first choice.

For all following analyses of event determination the simple linear examples of chapter 1 are used. The signal sequence can be described with equation 2. n stands for an offset which is assumed to be 0, except by the time jitter contemplation in figure 1 c. The searched time stamp for the LED method is according to equation 3. By assuming small and normal distributed effects, the Gaussian error propagation (equation 4, [6]) can be applied to study the qualitative influences. The complete result of the standard deviation of the time stamp is calculated in equation 5, the trigger threshold A_{th} is here assumed to be constant. With equation 5 can be interpreted, that an acquired time stamp depends on variable amplitudes, variable rise times and noise. Further three interesting things can be recognised. First: A faster threshold crossing $m_{T_{LED}}$ minimise all three effects. Second: A lower threshold $\frac{A_{th}}{A}$ is reducing the time walk effect. Third: σ_n is inversely proportional to $m_{T_{LED}}$.

$$y(t) = \frac{A}{T_R}t + n \tag{2}$$

$$T_{LED} = \frac{(A_{th} - n)T_R}{A} \tag{3}$$

$$\sigma_f = \sqrt{\sum_i \left(\frac{\partial f}{\partial x_i}\sigma x_i\right)^2} \tag{4}$$

$$\sigma_{T_{LED}} = \sqrt{\left(\frac{A_{th}}{m_{T_{LED}} \cdot A} \cdot \sigma_A\right)^2 + \left(\frac{A_{th}}{A} \cdot \sigma_{T_R}\right)^2 + \left(\frac{\sigma_n}{m_{T_{LED}}}\right)^2} \tag{5}$$

A further procedure is the **leading edge discriminator in combination with a**

high-low-coincidence method. It can reduce the impact of varying signal amplitudes and the resulting time walk effect [7]. The idea is the application of two trigger thresholds instead of one, a low and a high one. The low threshold is reducing the time walk as described before (figure 1 a, b). The high threshold is reducing or eliminating the failure rate of detected events caused by noise amplitudes. After the low threshold is crossed, a coincidence timer starts and the time stamp will stored temporary. If a crossing of the high threshold occurred still before the end of the coincidence time, the stored time stamp is validated.

The idea for a **constant fraction discriminator (CFD)** is an optimum triggering fraction for leading edge timing. The main goal is the reduction of the time walk [8]. A reduction of time jitter by means of a corresponding realisation is possible too. The special feature of the CFD is the independence of the signal amplitude for time event detection. This method generates an output without a constant trigger threshold, rather with a proportional part of the maximum impulse amplitude. A minimum implementation of a CFD is shown in figure 2. The signal is routed in two lines. One makes a delay and the other a attenuation and inversion. Then both are added. The configuration parameters are the attenuation factor $0 < c < 1$ and the delay time $\tau < T_R$. The zero crossing of the output signal stands for the acquired time stamp.

Two cases has to be considered for CFD implementation. One is the **true-constant-fraction timing (TCF)** and the second is the **amplitude-rise-time-compensated timing (ARC)** [1].
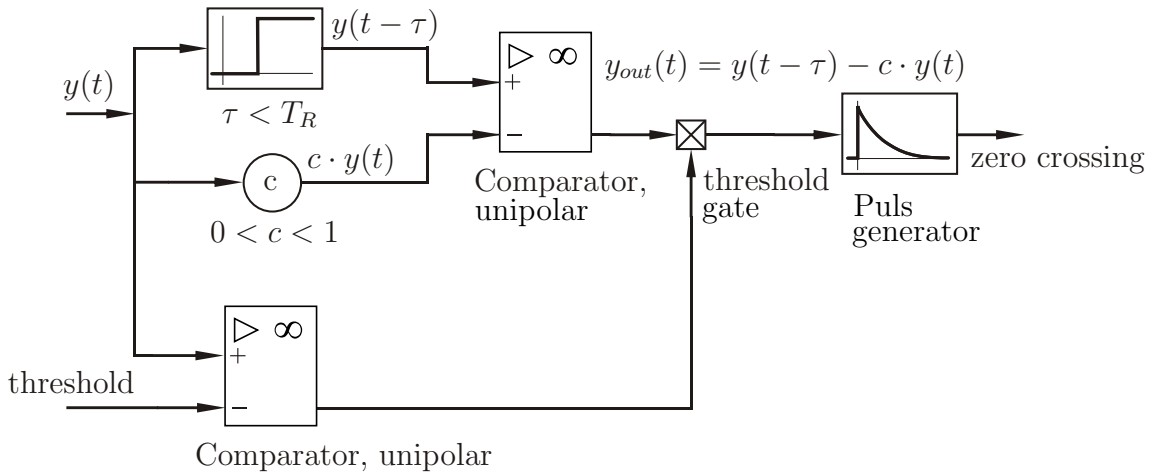

Figure 2: Constant fraction discriminator [1]

The **TCF** method can minimise the effects of variable signal amplitudes. Further it is possible to minimise the effects by noise. For that the slopes of the both CFD signals have to be the same slope polarity at zero crossing of y_{out} (figure 3: left side). The resulting time stamp is always $T > T_R$. Furthermore the generation of output signals for variable input amplitudes is shown in figure 4. There is to recognise, that the generated zero crossings are always at the same time. The time stamp can be calculated with equation 6. The equation shows that the detected time stamp is no longer dependent on the amplitude A.

The configuration parameter τ_{TCF} can now be determined in equation 7. The complete standard deviation of the detected time stamp with TCF method is shown in equation 8, where $\sigma_{n_{TCF}}$ is the resulting noise, $m_{T_{TCF}}$ is the resulting signal slope at zero crossing, c is the attenuation factor and σ_{T_R} is the standard deviation for signal rise times.

$$T_{TCF} = \frac{2 \cdot c \cdot T_R + \tau_{TCF}}{c + 1} \tag{6}$$

$$\tau_{TCF} > T_R(1 - c) \tag{7}$$

$$\sigma_{T_{TCF}} = \sqrt{\left(\frac{2 \cdot c}{c + 1} \cdot \sigma_{T_R}\right)^2 + \left(\frac{\sigma_{n_{TCF}}}{m_{T_{TCF}}}\right)^2} \tag{8}$$

As already mentioned equation 8 shows, that the TCF measurement accuracy is no longer influenced by the signal amplitude. Only two factors remain, the rise time and the noise. The new CFD noise $\sigma_{n_{TCF}}$ (equation 9) is now inversely proportional to the resulting increase $m_{T_{TCF}}$ from the CFD (equation 10). The difference between the noise of the LED and the TCF method is described by the factor $\frac{\sqrt{1+c^2}}{1+c}$, where the result is always smaller than 1 with $0 < c < 1$. For this it follows that $\sigma_{n_{LED}} > \sigma_{n_{TCF}}$.

$$\sigma_{n_{TCF}} = \sigma_n \sqrt{1 + c^2} \tag{9}$$

$$m_{T_{TCF}} = m_{T_{LED}}(1 + c) \tag{10}$$

The advantage of the **ARC** method is the capability to minimise the influence both of variable amplitudes **and** variable rise times. The disadvantage is a larger noise sensitivity than this of LED and TCF methods [1]. The reason is the different slope polarity of the two CFD signals at the zero crossing of y_{out} because the acquired time stamp is always $T < T_R$. The working principle is shown in figure 3: right. The time stamp for the ARC method is determinable with equation 11. There is to identify, that the time stamp is not dependant on the amplitude or the rise time but only of the CFD configuration parameters c and τ_{ARC}. Now τ_{ARC} can be described with equation 12, where $T_{R_{min}}$ is the minimal expected signal rise time. When the configuration parameters are assumed to be constant, the standard deviation of each detected time event is described with equation 13.

$$T_{ARC} = \frac{\tau_{ARC}}{1 - c} \tag{11}$$

$$\tau_{ARC} < T_{R_{min}}(1 - c) \tag{12}$$

$$\sigma_{T_{ARC}} = \frac{\sigma_{n_{ARC}}}{m_{T_{ARC}}} \tag{13}$$

There again can be seen, that for using ARC methods an acquired time stamp is only dependent on noise. The ARC noise $\sigma_{n_{ARC}}$ is equal to the TCF noise $\sigma_{n_{TCF}}$ (equation 9) but the slope at zero crossing is

$$m_{T_{ARC}} = m_{T_{LED}}(1 - c) \tag{14}$$

A difference between the noise for LED and ARC methods with the factor $\frac{\sqrt{1+c^2}}{1-c}$ follows, which is always larger than 1 by $0 < c < 1$. In summary it is possible to achieve these influences of noise for corresponding realisation:

$$\sigma_{n_{TCF}} < \sigma_{n_{LED}} < \sigma_{n_{ARC}} \tag{15}$$

Table 1 shows a qualitative summary of the analysed procedures.

LED	TCF	ARC
$\sigma_{T_{LED}} = f(\sigma_A, \sigma_{T_R}, \sigma_n)$	$\sigma_{T_{TCF}} = f(\sigma_{T_R}, \sigma_n \cdot \frac{\sqrt{1+c^2}}{1+c})$	$\sigma_{T_{ARC}} = f(\sigma_n \cdot \frac{\sqrt{1+c^2}}{1-c})$

Table 1: Qualitative standard deviation of time stamps for different edge detection methods
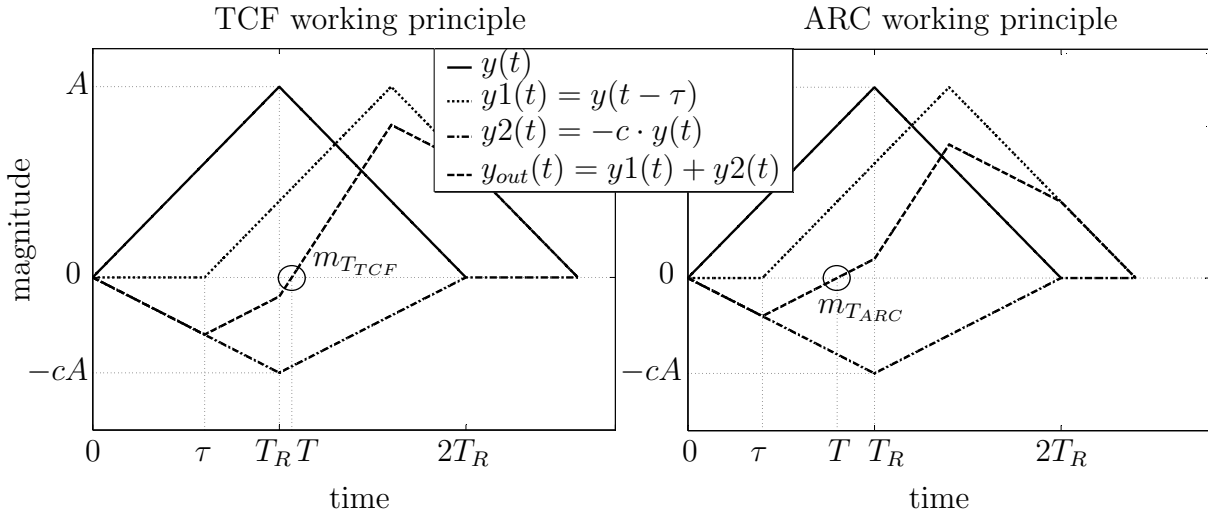

Figure 3: The both CFD working principles shows different slopes at zero crossing

3 Short description of the measurement assembly and application

As an application a procedure to measure the blade twist on axial compressors was used to determine its operation point. For this at least two compressor blade sensors and at least one encoder wheel sensor are required (figure 5). The two blade sensors have a vertical alignment to detect the blade crossings, here called leading and trailing edge. A blade twist appears subject to load or difference pressure over a compressor stage and can be gauged. By means of measuring the time difference Δt between the blade-sensor
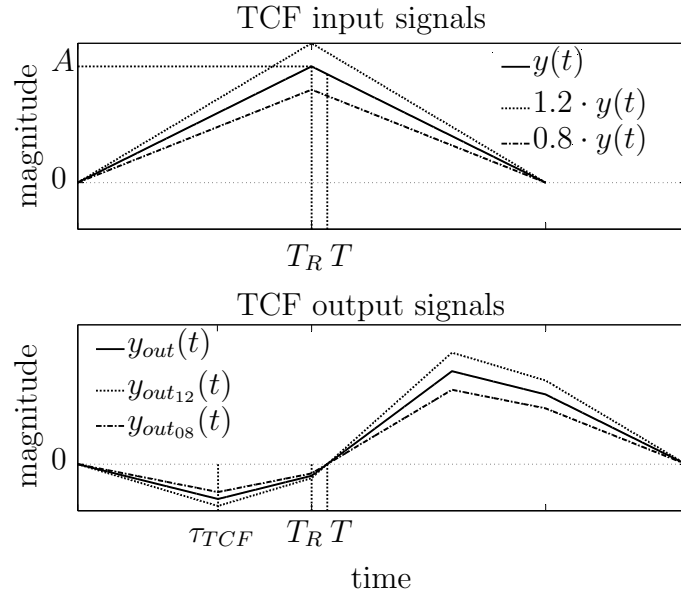
Figure 4: TCF output signals for variable input amplitudes

crossings of each sensor. With the time difference and the current revolution time, which is measured by the wheel sensor, it is possible to conclude to a blade twist. This method is based on [9]. In addition, there are further detailed physical explanations. This paper is concentrated on the measurement task and not to the physical interpretation or control strategies.
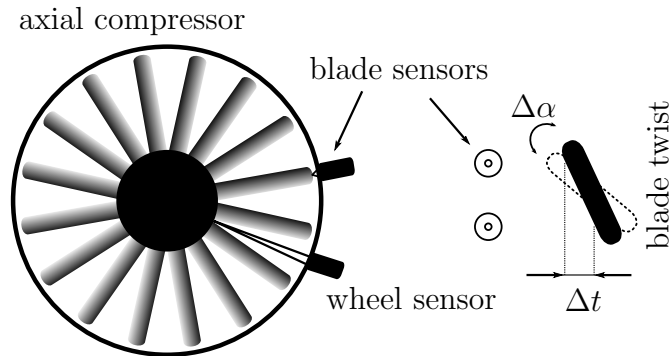

Figure 5: Principle for blade twist measuring on compressors

In this investigation laser transceivers ($\lambda \approx 785 \ nm$, $P \approx 25 \ mW$, $d_{fibre} \approx 5 \ \mu m$) basing on Si-Photodetectors (THORLABS DET02AFC) were used. Their signals are sampled with a digital storage oscilloscope with a sample rate of $250 \ MHz$ per channel. For the investigation a compressor with 20 blades and a diameter of approximately $0.5 \ m$ was used. For a circumferential speed of $48 \ \frac{m}{s}$, which corresponds to a rotational speed of $1800 \ rpm$, a measurement resolution of $0.19 \ \mu m$ by $4 \ ns$ can be achieved. It is to be noted, that the storage capability of the oscilloscope is very limited. Hence it was possible to store approximately one rotor revolution. Due to this reason nearly all following investigations were done with single measurements, consequently without averaging. Furthermore, the estimation of measurement accuracy with the present data is not possible.

The direct usage of the sampled signals minimise the influence of further processing steps. This way it is possible to prevent loss information, which occurs by digitising

the signals with a leading edge discriminator after gaining them. No information will be available in this case to interpret the quality of each acquired time event. However, in further development steps this method is not excluded. In figure 6 an example of the unfiltered values from channel 1 and channel 3 of the digital storage oscilloscope is shown. The channels each represent the leading and trailing edge of the compressor blades. Both plots show the same compressor blades in two measurements in series. The first measurement is recorded at the experiment's maximum load, which is not the compressor maximum load. The second measurement is recorded at a smaller load. It can be recognised first, that there is a strong potential for a time walk effect and second that there will be problems by the clear detection of time events. To first: Nearly all blade signals have different maximum amplitudes, particularly those at sample position $3.8 \cdot 10^6$ and $4.2 \cdot 10^6$. This effect will result in different slew rates in each revolution. When using a common leading edge discriminator with a constant threshold, the detection time of blade x will therefore vary in each revolution. To second: Channel 3 doesn't have optimal signal quality. The sampled blade at position $3.6 \cdot 10^6$ shows two rising edges and thus two potentially detected time events. This should be prevented.
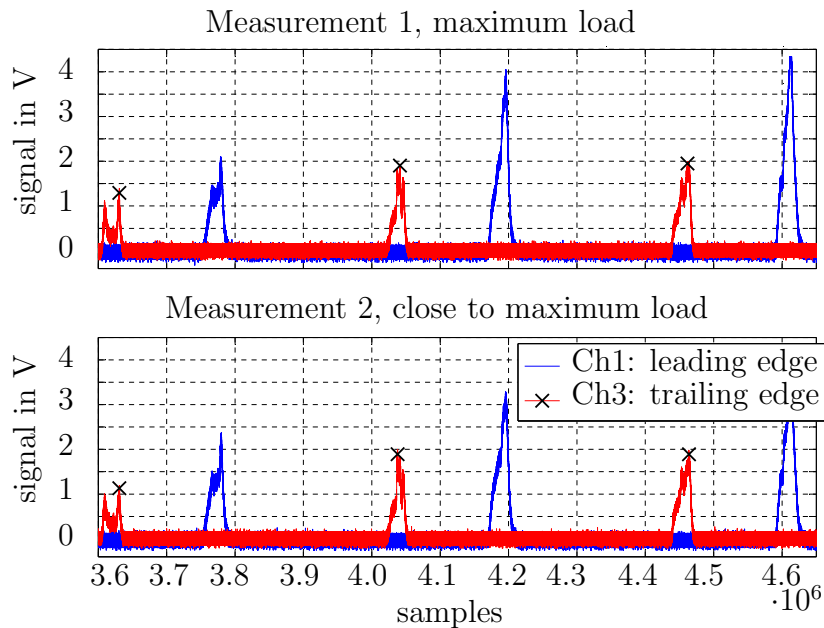

Figure 6: Signal example of measurements 1 and 2, raw signals of photo detectors

For this measurement task a special algorithm was developed (figure 7). It includes a constant fraction discriminator (CFD: TCF), an average filter and a coincidence timer with logic. These parts reduce the time walk and time jitter effects and eliminate false or multiple detected time events. After a zero crossing is detected the corresponding time stamp is stored temporary and the the coincidence timer starts. The timer has two outputs. One output generates a logic high for a defined time T_s. Within this time the signal $y_{f_{out}}$ is checked for further zero crossings. If this case occurs the temporary time stamp is deleted. The second output locks the time stamp detection for a defined time

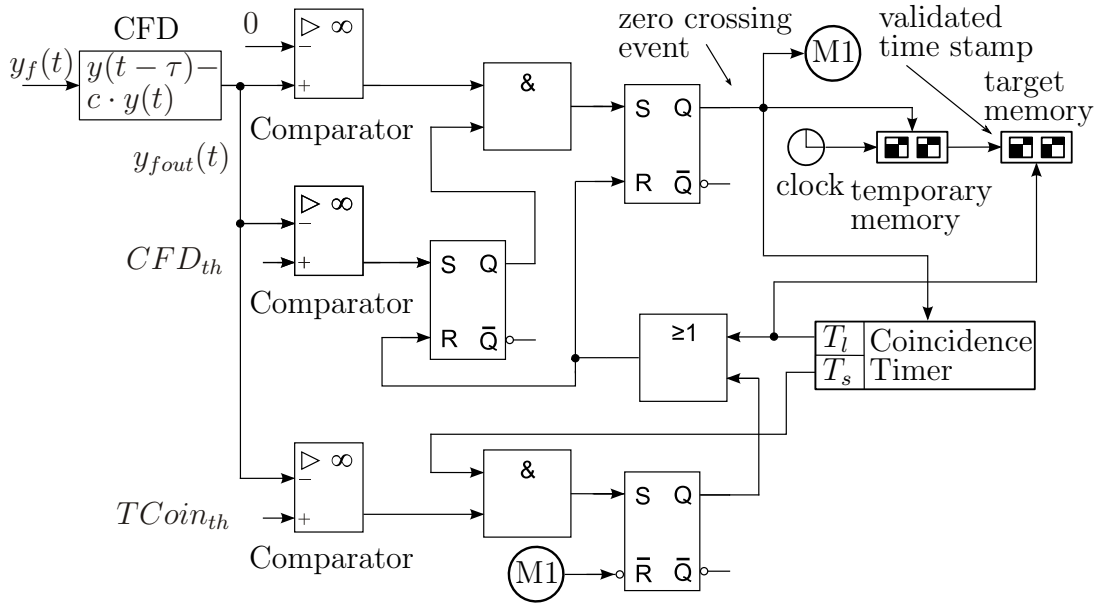$T_l > T_S$. After the time ran out the temporary time stamp becomes valid (figure 8: crosses).

Figure 7: Time event detection algorithm for one channel, without average filter

In figure 8 an example of the output for the implemented CFD method in combination with a average filter with 10 coefficients is shown. The zero crossings represent acquired time events. Channel 1 has relative good signal quality and the resulted slope at crossing zero is relatively steep and clear. Not so on channel 3, there are no clear time events. As already written, the blade signal at position $3.6 \cdot 10^6$ contains two slopes. Furthermore at position $4.05 \cdot 10^6$ an event is detected by mistake. These events will be eliminated by the described developed algorithm.
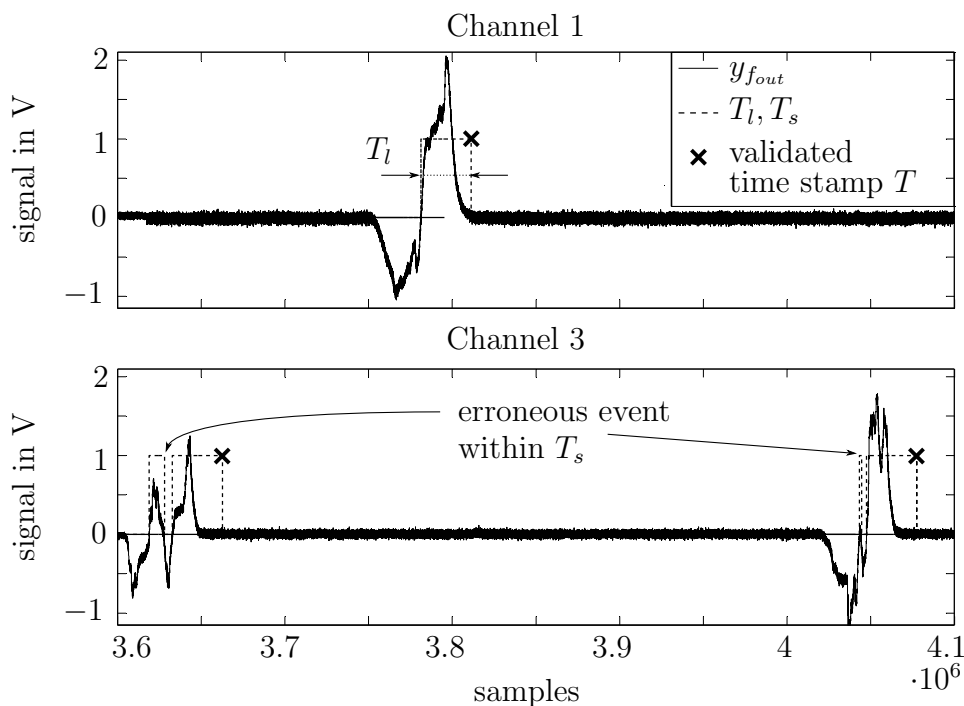

Figure 8: CFD method and average filter with measurement 1: channel 1 and 3

4 Evaluation of the measurement results

For the evaluation, sampled signals from 9 measurement records were used. The compressor load was reduced stepwise from the experiment's maximum to minimum by opening a throttle step by step.

In figure 9 (a) the time delay profiles of the measurement records 1 to 9 (full load to closely idle) can be seen. These profiles represent the measured time between the trailing and leading edge. It shows the very good measurement repeatability without averaging. Nearly each blade has its individual distance from trailing to leading edge. Blade 4 has one measurement outlier. This will be removed in further figures.

(a) Time delay profiles (interpolated) for leading and trailing edges of each measurement record

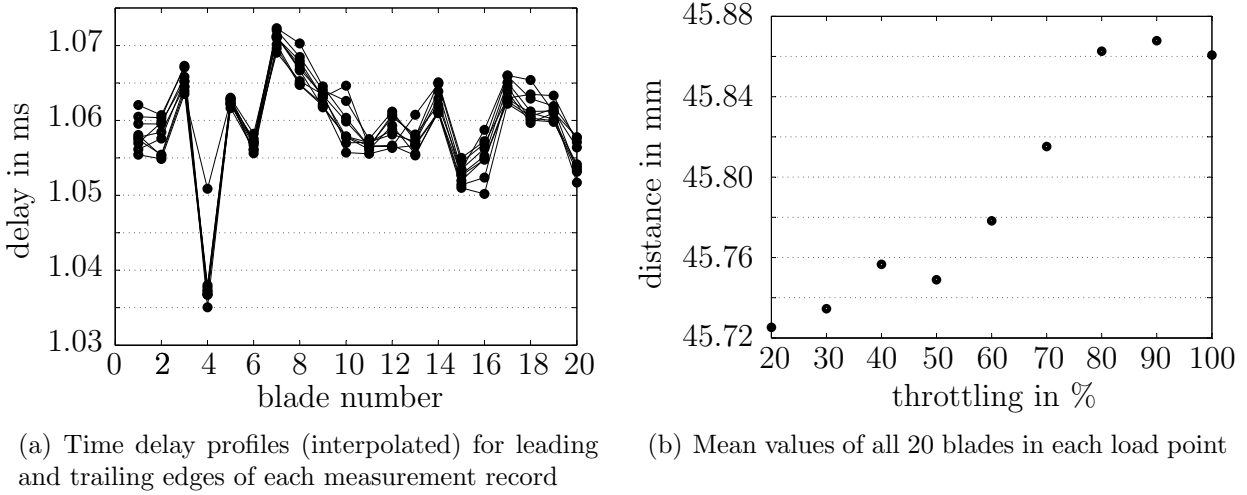(b) Mean values of all 20 blades in each load point

Figure 9: Measurement results

A more detailed presentation for the distance profiles can be seen in figure 10, with 20 plots, each for one blade, with measured and calculated distances (blue crosses) from maximum load to closely idle (measurements 1 to 9). **It is to consider, that 17 of 20 blades indicate a blade twist in dependence of load**. Currently there is no verified explanation for behaviour of the four blades (4, 5, 12) without a blade twist. One reason could be a too high standard deviation, because each value represents only one measurement. Another reason could be a variable blade stiffnesses. Furthermore, there is at present no explanation for the strong different gradients (red lines). Again the reasons for this could be different blade stiffnesses or inadequate measurement accuracy.

The distance in meters can be calculated with the equations 16 and 17. $Tdiff$ stands for the calculated time delay of each blade. $Tref$ is the measured time event of the reference signal, it can be chosen freely. $Tblade$ is the measured signal to be compared with the reference, r is defined as the number of compressor blades, a_i is the distance for each blade, u is defined as the compressor circumference and Tn stands for the current revolution time. The index i represents the blade number from 1 to r and k indicates the number of the measured time event. As described before, the oscilloscope memory is limited to a maximum of 24 time events per channel and measurement record. For this reason it is only possible to calculate four Tn values per measurement record. The

average of these four values is used to determine the distances.

$$Tdiff_i = Tref_i - Tblade_i \text{ for } 0 < i < r + 1 \tag{16}$$

$$a_i = \frac{Tdiff_i}{Tn_i(k)} \cdot u = \frac{Tdiff_i}{Tref_i(k) - Tref_i(k-r)} \cdot u \tag{17}$$
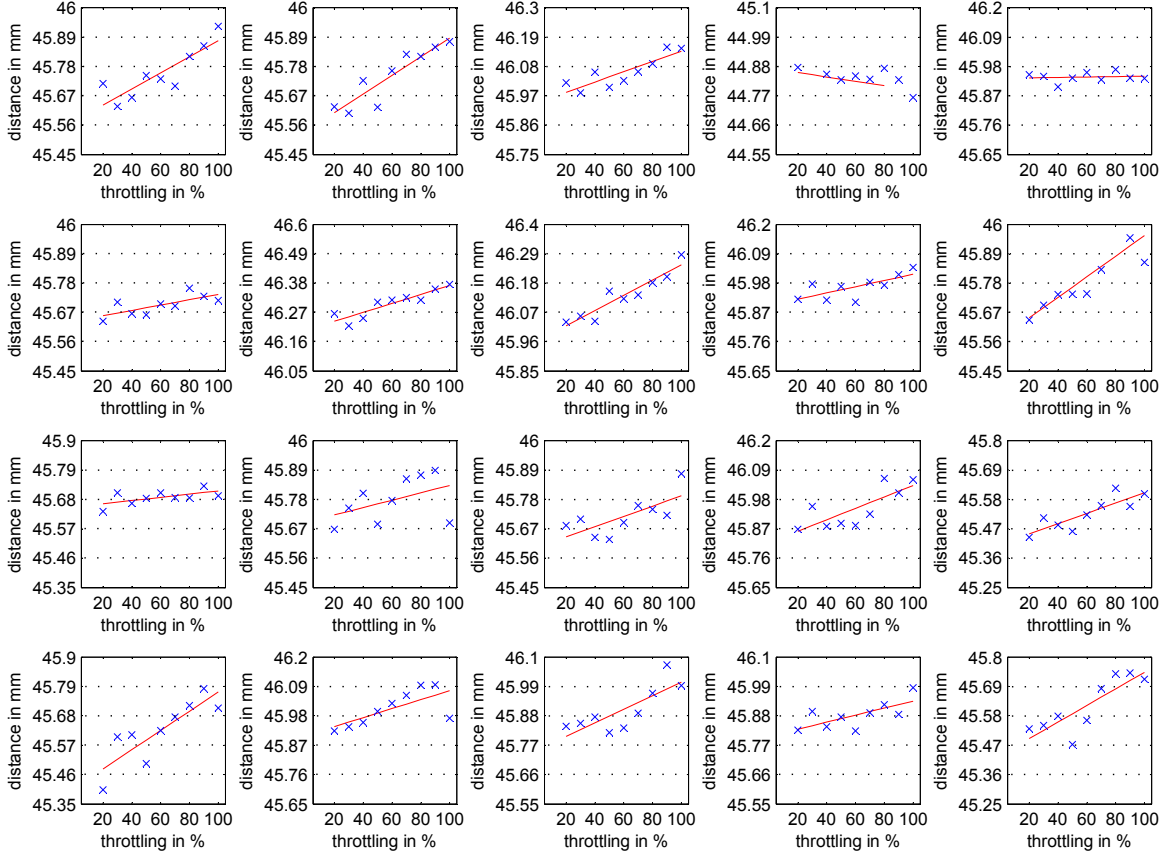

Figure 10: Distances of blades 1 to 20 in relation to measurement record 1 to 9, reading from left to right and up to down

In Figure 9 (b) the mean values of the calculated differences of all 20 blades in each load point (measurement records 1 to 9) are shown. The measurement outlier of blade number 4 in measurement series 8 is removed. A delay and a saturation in blade twisting can be recognise. A similarity with throttle curves can as well be identified. Further explanations could be too low loads, a too long time constant of the process to notice an effect or inadequate measurement accuracy. Currently the actual reason has to be investigated. Furthermore is to be noted, that values in figure 9 (b) are no longer single shot measurements, but averaged values. Now there is an averaging of 20 values (number of blades) in each load point. The variation of distances from leading to trailing edge can be interpreted with the help of the cosine from the unit circle. The blade twist starts at a large cosine value at full load and proceeds to a smaller cosine value at idle, or the blade twist starts at an approximately horizontal position at full load and proceeds to a position with a larger vertical alignment. The maximum twist is approximately 100 μm at this constellation.

5   Conclusion

Summarised the measurability of blade twisting on axial compressors can be determined with this principle. Furthermore there is a great potential to improve the measurement assembly and to gain the accuracy and availability. Thinkable are alternative sensor principles and at least two different detection variants for online analysis. The first variant may base on fast ADCs sampling the signals and analysing them directly in the data streams, like CFD or correlation. For this purpose field programmable gate arrays (FPGA) will be probably the best way to use . This variant would be similar to the described offline analysis of this paper. The second variant is the application of discrete built CFDs as analogue circuits and the detection of the time events by means of a micro controller. Here the main challenge would be the implementation of variable or adaptive CFDs. The advantage here is the renunciation of more expansive ADC's. Conceivable are also hybrid systems of the two variants, for example discrete CFDs and FPGA without ADCs.

References

[1]   Paulus, TJ: Timing electronics and fast timing methods with scintillation detectors. In: *Nuclear Science, IEEE Transactions on* 32 (1985), Nr. 3, S. 1242–1249

[2]   Spieler, Helmuth: *Semiconductor detector systems.* Oxford university press, 2008

[3]   Packard, Hewlett: Time Interval Averaging. In: *Application Note 162-1* 1 (1970), S. 16

[4]   Henzler, Stefan: *Time-to-Digital Converters.* Springer, 2010

[5]   Kalisz, Josef: Review of methods for time interval measurements with picosecond resolution. In: *Metrologia* 41 (2003), S. 16

[6]   Lerch, Reinhard: *Elektrische Messtechnik.* Springer Vieweg, 2012

[7]   *SAPHIR - Ein Mittelenergie-Experiment.* http://saphir.physik.uni-bonn.de. `http://saphir.physik.uni-bonn.de/saphir/thesis/9424/diplom/node17.html`. Version: September 1997

[8]   Gedcke, DA ; McDonald, WJ: Design of the constant fraction of pulse height trigger for optimum time resolution. In: *Nuclear Instruments and Methods* 58 (1968), Nr. 2, S. 253–260

[9]   Köller, M. ; Magnor, O. ; Reitebuch, D.: *Device and method for reliably operating a compressor at the pump threshold.* `http://www.google.com/patents/EP2619461A1?cl=en`. Version: Juli 31 2013. – EP Patent App. EP20,110,813,656